Hydraulic Analogy Examination of Underexpanded Jet Shock Cells using Reference Image Topography

V. Kumar[1], I. Ng[1], G. J. Sheard[2], K. Hourigan[1,2] and A. Fouras[1,2]

[1]Division of Biological Engineering, Monash University, VIC 3800, Australia
fouras@eng.monash.edu.au

[2]Fluids Laboratory for Aeronautical and Industrial Research (FLAIR), Department of Mechanical and Aerospace
Engineering, Monash University, VIC 3800, Australia

ABSTRACT

This paper examines the shock cell structure at the exit of
an underexpanded jet nozzle using a hydraulic analogy. This
approach allows thorough investigation of this important flow
regime at a greatly reduced expense. Applying the novel
Reference Image Topography technique (Fouras *et al.* [1]),
the wavy water surface is reconstructed, providing a pressure
map of the nozzle exit region. This allows a detailed analysis
of the underlying shock cell structure and the flow instabilities
resulting in jet screech.

1. INTRODUCTION

The flow behind jet nozzles has been a matter of great interest
due to its effects on the aerodynamics, structure and propulsion
system of an aircraft. The first shock cell formed at the exit
of an underexpanded jet nozzle provides valuable information
regarding the flow properties, such as pressure variations,
exhaust velocity, acoustic vibrations, viscous effects, etc. A
thorough understanding of pressure distribution at the exit of
the nozzle can assist in various studies, such as the investigation
of screech phenomenon that is potentially harmful for aircraft
bodies (Brocher *et al.* [2]; Buchanan *et al.* [3]), and enhanced
mixing for combustion applications (Alkislar *et al.* [4]; Alkislar
et al. [5]). A nozzle is said to be underexpanded when the
ambient atmospheric pressure is lower than the pressure at the
nozzle exit, which implies the flow at the exhaust is capable of
further expansion.

The technique used to visualise this flow is based on the concept
of comparing a reference image and the same image through a
distorted surface to produce apparent displacement vectors that
can be used to reconstruct the surface topography. Inherently,
this is a simple, cost-effective and highly accurate technique.

2. THE HYDRAULIC ANALOGY

According to the hydraulic analogy, the free-surface topography
of water on a water table relates to the pressure, temperature
and density profiles, while the velocity field is directly related
to vorticity in the flow (Buchanan *et al.* [3]; Fouras *et
al.* [6]). The hydraulic analogy is useful for simulating
high-speed 2D compressible ideal gas flow with shallow water
flow (Buchanan *et al.* [3]). The study of high-speed jet flows
becomes much simpler, more convenient and accurate, as the
wave propagation and flow speed is three orders of magnitude
slower than gas flow. Differences in pressure, temperature and
density in gas flow correspond to differences in water depth
across a converging nozzle placed on the water table. The
Froude number, *Fr*, in the water is considered analogous to
the Mach number, *Ma*, for gas flow (Buchanan *et al.* [3]),

subsequently allowing the pressure ratio across the nozzle to
determine the equivalent speed of the gas (White [7]). Dynamic
equivalence between the two flows is thus achieved by a simple
manipulation of equations (as in (1) and (2)).

$$Ma \equiv Fr = \left[2 \left(\frac{h}{h_0} - 1 \right) \right]^{\frac{1}{2}} \ldots \gamma = 2, \tag{1}$$

$$\frac{p}{p_0} = \left[1 + \frac{1}{2}(\gamma - 1)Ma^2 \right]^{\frac{\gamma}{\gamma-1}} \ldots \gamma = 2, \tag{2}$$

where γ is the specific heat ratio, h is the water depth in the
upstream reservoir and h_0 is the mean water depth in the test
section. A summary of the hydraulic analogy is provided in
Table 1 (Buchanan *et al.* [3]).

Table 1: Analogous equations and variables for two
dimensional gas and shallow hydraulic flows.

Gas flow	Hydraulic flow	Implication
$\frac{T}{T_0} = 1 + \frac{\gamma-1}{2}Ma^2$	$\frac{h}{h_0} = 1 + \frac{1}{2}Fr^2$	$\frac{T}{T_0} \equiv \frac{h}{h_0}; \gamma = 2$
$\frac{\partial}{\partial x}(\rho u) + \frac{\partial}{\partial y}(\rho v) = 0$	$\frac{\partial}{\partial x}(hu) + \frac{\partial}{\partial y}(hv) = 0$	$Ma \equiv Fr;$ $\frac{\rho}{\rho_0} \equiv \frac{h}{h_0}$
$\frac{p}{p_0} = \frac{\rho}{\rho_0}\frac{T}{T_0}$		$\frac{p}{p_0} = \left(\frac{h}{h_0}\right)^2$

It is worth noting that the analogy does not provide a direct
quantitative representation of aerodynamic flows in air, but
rather that of a hydraulic gas in which γ is 2. However, this
restriction can be neglected as most relevant experiments will
have insignificant influence of varying γ (Buchanan *et al.* [3]).

3. FLOW VISUALISATION

3.1 Technique

The technique used in this paper is based on the Reference
Image Topography technique described in Fouras *et al.* [1].
A converging perspex nozzle is placed on a glass-bottomed
water table, through which shallow water flows at a steady rate.
A ground glass plate, used as a reference object, is attached
underneath the glass bottom in the region of the shock cell. The
camera's frame of view (105 mm streamwise $\times$ 85 mm lateral
= 1024 pixels $\times$ 826 pixels) encompasses the entire first shock
cell. A light source (300 W halogen lamp), collimated by a
long aspect ratio box lined with a reflective surface, is used
to illuminate the semi-translucent reference object. A similar
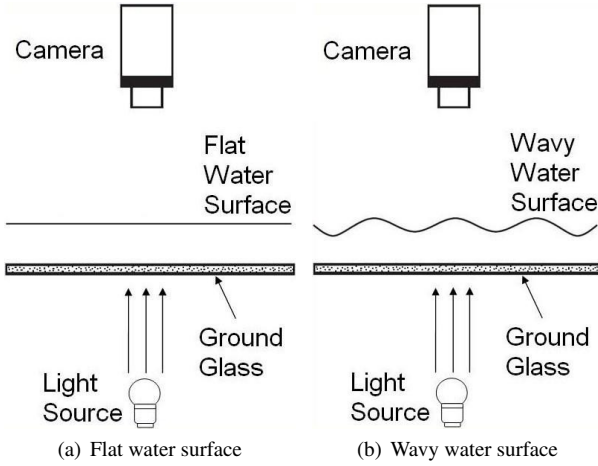technique was employed by Moisy *et al.* [8].

(a) Flat water surface (b) Wavy water surface

Figure 1: Schematic of the configuration of the camera, ground glass and light source with respect to the water surface (adapted from Fouras *et al.* [6]). The glass is illuminated from below, with the light rays passing through the glass and water to reach the camera after refraction at the water-air interface.

Images of the ground glass resemble those of a dense set of particles, which are used as a reference image through still water. As water flows through the nozzle, the disturbed surface distorts the reference image. Comparing the reference image with this distorted image, a grid of apparent displacement vectors is produced. With appropriate analysis using the height estimation algorithm (described below), these vectors can be used to reconstruct the topography of the distorted surface. This visualisation technique allows for any study that requires the accurate measurement of surface topography in a simple, cost-efficient and repeatable manner (Fouras *et al.* [1]).

3.2 Height Estimation Algorithm

The apparent displacement vectors (δ_x, δ_y) relate to the free-surface gradients ($\partial H/\partial x$ and $\partial H/\partial y$), which can be integrated by an algorithm to estimate the water height distribution (Fouras *et al.* [6]). The mean water height, set as the reference height (H_{ref}), is taken as the initial height estimate, H. Based on the configuration in Figure 2 and using Snell's law of refraction at the water-air interface ($\eta_{air} \sin\alpha_1 = \eta_{liquid} \sin\alpha_2$), the relationship to estimate $\partial H/\partial x$ and $\partial H/\partial y$ using the current guesses of H is derived as (Fouras *et al.* [6]):

$$\tan^{-1}\frac{\delta_x}{H} = \tan^{-1}\frac{\partial H}{\partial x} - \sin^{-1}\left[\frac{\eta_{air}}{\eta_{liquid}}\sin\left(\tan^{-1}\frac{\partial H}{\partial x}\right)\right]. \quad (3)$$

Integrating $\partial H/\partial x$ and $\partial H/\partial y$ yields the estimated heights, H_{est}, which can be adjusted to give H_{adj} by applying a minimum-error approach between measured displacements and reference image particle positions. An iterative process is applied until the value of H_{adj} converges. A detailed description of the height-solving algorithm is contained in Fouras *et al.* [6]. As the distance of the camera from the glass table is much greater than the thickness of the glass bottom and the angle of refractions at the glass-air and glass-water interfaces are very small, the refraction effect of the glass bottom can be neglected (Moisy *et al.* [8]).

3.3 Shock Cells

In the 2D visualisation of Figure 3, the nature of the jet shock cells in a supersonic flow regime can be seen. A series of expansion waves are formed at the nozzle exit that propagate until they reach the jet shear (boundary) layer. Here
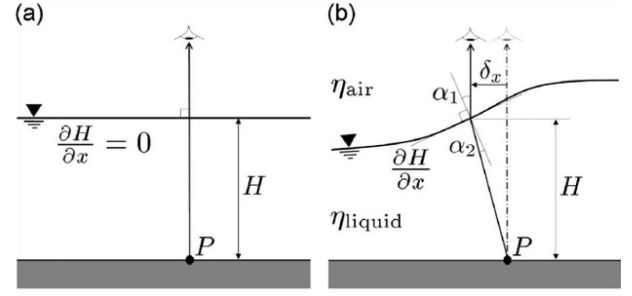

Figure 2: Geometry and nomenclature for the height estimation algorithm. (a) Undistorted position of point *P* through an undisturbed surface (b) Apparent displacement δ_x of point *P* due to refraction through the surface at height *H* with gradient $\partial H/\partial x$. Refractive indices of the air η_{air} and liquid η_{liquid} phases are shown, as are the refraction angles α_1 and α_2 (Fouras *et al.* [6]).

they are reflected as compression waves and so on until the ambient pressure (or back pressure) is reached. This process of reflection of expansion and compression waves results in a diamond-shaped pattern being formed in the jet. Larger Mach numbers produce greater shock cell spacing.
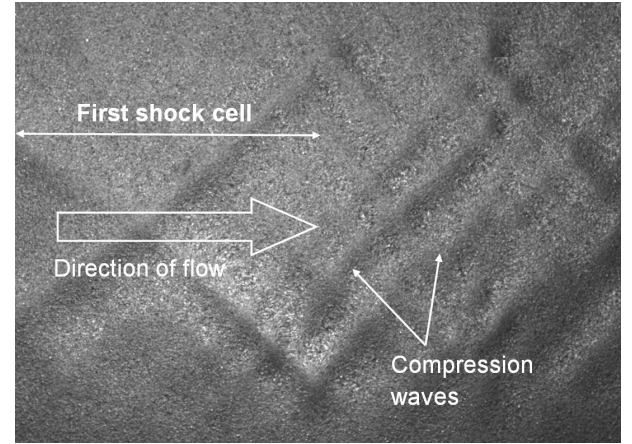

Figure 3: Shock cell and diamond-shaped pattern formed at nozzle exit in a supersonic flow regime, as seen by the camera from above. The particle-like nature of the ground glass gives the image a grainy look.

4. RESULTS

The upstream water depth was varied to control the pressure ratio and hence the resulting Mach number (Table 1). A low downstream water depth was chosen to produce well-defined shock cells with relatively low surface gradients for effective height estimation. An interrogation window size of 16 pixels × 16 pixels was chosen to provide high accuracy and effective vector correlation in an efficient manner.

4.1 Time-averaged

The time-averaged surface reconstruction for early-development shock cells is shown in Figure 4. The harmonics are clearly evident in the reconstruction, with greater pressure gradients visible at the shock cell corners. The time-averaged surface displays flat edges in the jet shear layer along the side of the shock cells, while the shock cells remain stable and steady in shape. A gradual decay in the strength of the shock cells can be observed with distance downstream.
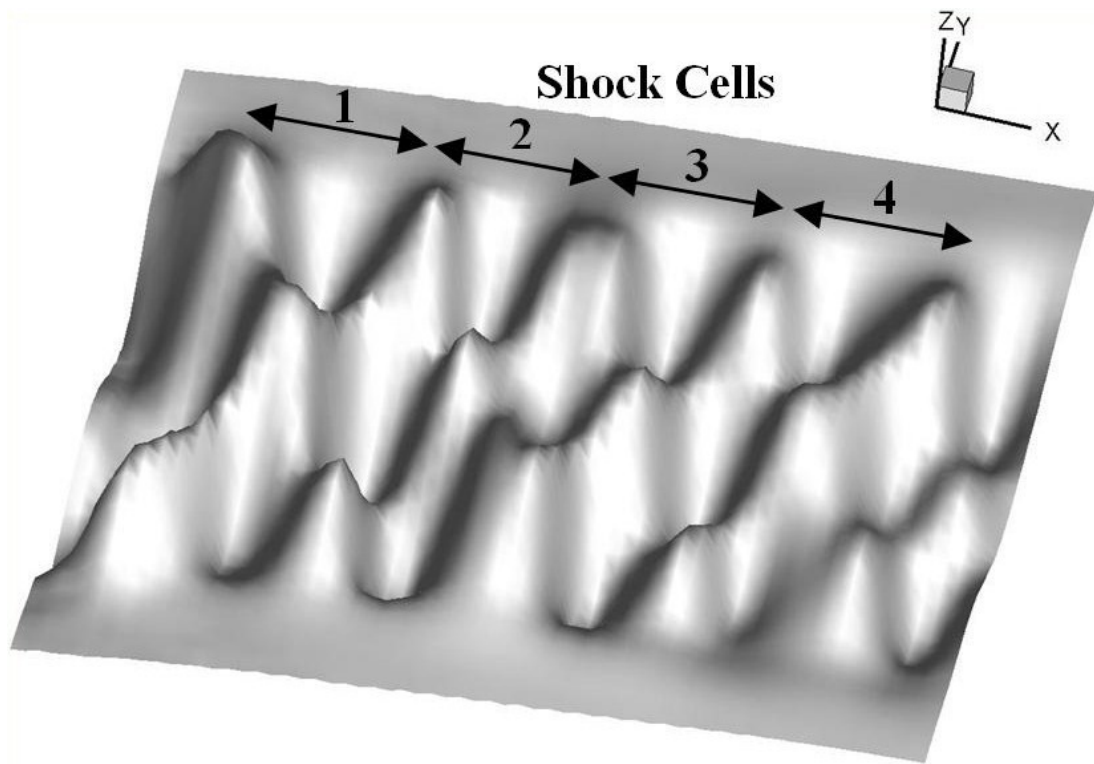
Figure 4: Time-averaged surface reconstruction of the shock cells. The variation in water surface height in the region of the first four shock cells is distinct.
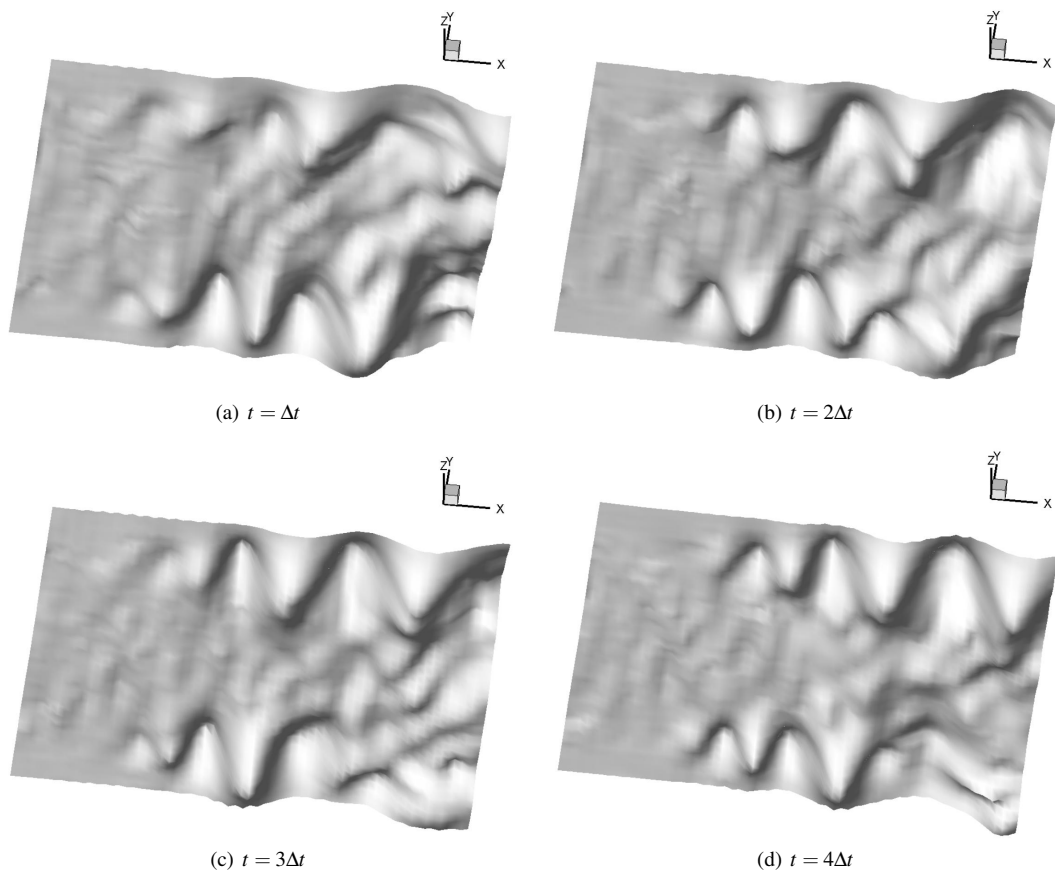

(a) $t = \Delta t$

(b) $t = 2\Delta t$

(c) $t = 3\Delta t$

(d) $t = 4\Delta t$

Figure 5: Downstream propagation of vortices along jet shear layer on either side of shock cells. The vortex structures can be seen to increase in size and strength as they propagate downstream. $\Delta t = \frac{1}{14}$ s. A relatively stable surface is observed near the nozzle exit, while interaction between shock cells and vortices downstream creates instabilities. Flow is from left to right.

4.2 Temporal

The time-averaged surface (Figure 4) is subtracted from the instantaneous surfaces to highlight the non-steady regions of the flow. This is shown in Figure 5, where periodic vortices propagate downstream on either side of the shock cells. Over time, these vortices are averaged to the mean water height, as exhibited by the flat regions in Figure 4. It is hypothesised that these vortex structures pump fluid into and out of the jet shear layer (Woodmansee *et al.* [9]).

These vortex structures originate from Taylor-Görtler instabilities caused by the concave curvature in the streamwise direction around the first shock cell in the expanding jet (Woodmansee *et al.* [9]; Schlichting *et al.* [10]; Smits *et al.* [11]). This is well in agreement with the results, where the vortices can be seen to originate from the first shock cell and the vorticity increases in strength downstream. Interaction between the larger vortices and shock cells downstream produces instabilities in the central flow region, which can be linked to the generation of acoustic power at the screech frequency (Buchanan *et al.* [3]). The strength of these vortices is purported to be related to the screech-tone intensity (Alkislar *et al.* [4]). The aeroacoustic phenomenon of screech, being potentially harmful for aircraft bodies, is an area of continual research and investigation (Buchanan *et al.* [3]; Alkislar *et al.* [4]).

5. CONCLUSIONS

The shock cell structure at the exit of an underexpanded jet nozzle has been analysed using the hydraulic analogy. Using the Reference Image Topography technique, the topography of the water was reconstructed. Vortices were observed to propagate downstream on either side of the shock cells with interaction downstream as the vortices grew in size. The variation in water height is intimately related to the pressure, temperature and density fields of the flow, which play a significant role in relevant fluid mechanics, jet propulsion and aircraft structural studies. The technique employed is relatively simple, cost-efficient, accurate, of superior image quality and easily repeatable (Fouras *et al.* [1]). Further work in analysing the velocity and vorticity distributions in the region, together with the pressure and temperature distributions, will provide a better understanding for the development of appropriate control measures for jet screech.

REFERENCES

[1] Fouras, A., Hourigan, K., Kawahashi, M. & Hirahara, H. (2006) An Improved, Free Surface, Topographic Technique, *Journal of Visualization*, **9(1)**, 49–56.

[2] Brocher, E. & Makhsud, A. (1997) A New Look at the Screech Tone Mechanism of Underexpanded Jets, *European Journal of Mechanics, B/Fluids*, **16(6)**, 877–891.

[3] Buchanan, A., Macartney, R., Thompson, M.C., Brocher, E. & Hourigan, K. (2007) Hydraulic Analogy Study of Supersonic Rectangular-Jet Screech Control with Cylinders, *AIAA Journal*, **45(7)**, 1539–1545.

[4] Alkislar, M.B., Krothapalli, A. & Lourenco, L.M. (2003) Structure of a Screeching Rectangular Jet: A Stereoscopic Particle Image Velocimetry Study, *Journal of Fluid Mechanics*, **489**, 121–154.

[5] Alkislar, M.B., Krothapalli, A. & Butler, G.W. (2007) The Effect of Streamwise Vortices on the Aeroacoustics of a Mach 0.9 Jet, *Journal of Fluid Mechanics*, **578**, DOI: 10.1017/S0022112007005022.

[6] Fouras, A., Lo Jacono, D., Sheard, G.J. & Hourigan, K. (2008) Measurement of Instantaneous Velocity and Surface Topography in the Wake of a Cylinder at Low Reynolds Number. *Journal of Fluids and Structures*, **24(8)**, 1271–1277.

[7] White, F.M. (1999) *Fluid Mechanics*, 4th edition, McGraw-Hill.

[8] Moisy, F., Rabaud, M. & Salsac, K. (2009) A Synthetic Schlieren Method for the Measurement of the Topography of a Liquid Interface. *Experiments in Fluids*, DOI: 10.1007/s00348-008-0608-z.

[9] Woodmansee, M.A., Iyer, V., Dutton J.C. & Lucht, R.P. (2004) Nonintrusive Pressure and Temperature Measurements in an Underexpanded Sonic Jet Flowfield. *AIAA Journal*, **42(6)**, 1170–1180.

[10] Schlichting, H. & Gersten, K. (2000) *Boundary Layer Theory*, 8th edition, Springer.

[11] Smits, A.J. & Dussauge, J. (2005) *Turbulent Shear Layers in Supersonic Flow*, 2nd edition, Birkhäuser.